ELSEVIER

Journal of Magnetism and Magnetic Materials 190 (1998) 98–107

Journal of magnetism and magnetic materials

Microscopic stress-induced magnetization changes in a fracture (1 1 1) surface of Terfenol-D observed with magnetic force microscopy

Jake Schmidt[a,*], Rob Tickle[b], George D. Skidmore[a], Chris Merton[a], Richard D. James[b], E. Dan Dahlberg[a]

[a]*Magnetic Microscopy Center, School of Physics and Astronomy, University of Minnesota, Minneapolis, MN 55455, USA*
[b]*Department of Aerospace Engineering and Mechanics, University of Minnesota, Minneapolis, MN 55455, USA*

Abstract

We have imaged mechanically polished and fractured (1 1 1) surfaces of Terfenol-D using magnetic force microscopy (MFM), and also the fracture surface during application of in situ applied stresses. The theory of James and Kinderlehrer (Phil. Magn. B 68 (1993) 237) has been used to explain some of the observed domain structures. Although some imaged domain structures are not predicted, there is general agreement with the theory. Observations indicate applied stress results in domain wall motion between existing domains as well as nucleation of new domains.

Keywords: Magnetization – stress-induced; Terfenol-D; Fracture surface

1. Introduction

Terfenol-D ($Tb_{0.3}Dy_{0.7}Fe_2$), because of its high magnetostriction to anisotropy ratio [1] ($\lambda_s \sim 2\times10^{-3}$, $K_1 \sim 2\times10^4$ erg/cm^3), is the subject of much technological and scientific interest. Bulk samples, which are typically float zone grown, characteristically contain growth twins. Numerous studies of magnetization and strain changes with applied field and stress have been carried out on twinned specimens [2–4]. Specifically, the work of James and Kinderlehrer [5] has predicted deformation and magnetic domain structures based on the self-compatibility of strains and magnetization in the microstructure of the material, including the effects of twinning. Various microscopies, such as optical, X-ray, and scanning electron microscopy, of different crystal surfaces have been used to observe the existence of surface deformations [6–9]. Atomic and magnetic force microscope (MFM) studies have also been used [10,11] to observe both deformation and magnetic domains. Here, we report the results of a series of MFM experiments on a fracture (1 1 1) surface of Terfenol-D with in situ applied stress. Images taken with no applied stress of both the polished and fracture surfaces were compared to James and Kinderlehrer's theory.

* Corresponding author. Fax: +1-612-624-4578; e-mail: schm0127@gold.tc.umn.edu.

0304-8853/98/$ – see front matter
PII: S0304-8853(98)00276-5

2. Theory

The phenomenon of magnetostriction relates changes in the strain of a material to changes in its magnetization. The application of stress to a magnetostrictive material induces an anisotropy with energy given by

$$E_\sigma = -\tfrac{3}{2}\lambda_s \sigma \cos^2\theta,$$

where λ_s is the saturation magnetostriction, σ the stress, and θ the angle the magnetization makes with the direction of the applied stress. Terfenol-D is a material with positive magnetostriction ($\lambda_s > 0$); if it is subjected to a tensile (compressive) stress, σ is positive (negative) and the magnetization has a low energy state lying parallel (in a plane perpendicular) to the stress axis.

Now, we consider the present experiment with the sample having an orientation described below with a compressive stress applied along the $[1\ 1\ \bar{2}]$ direction (see Fig. 1a for sample geometry). Including the effects of a magneto-crystalline anisotropy, there is one easy axis, the [1 1 1], which lies in the plane perpendicular to the stress axis. Of the remaining easy axis directions, ($[\bar{1}\ 1\ 1]$, $[1\ 1\ \bar{1}]$, and $[1\ \bar{1}\ 1]$), the $[1\ 1\ \bar{1}]$ axis makes an angle of 19.5° with the stress direction and the $[\bar{1}\ 1\ 1]$ and $[1\ \bar{1}\ 1]$ axes make angles of 61.5°. Therefore, the easy axis directions, listed from highest energy to lowest under a compressive stress, are $[1\ 1\ \bar{1}]$, $[\bar{1}\ 1\ 1]$ and $[1\ \bar{1}\ 1]$, and [1 1 1]. Therefore, under application of a compressive stress along this axis, we should expect to see the greatest changes to domains with easy axes in that order.

Because Terfenol-D is a magnetostrictive magnetic material, there is always a strain distribution present in the material associated with its remanent magnetic state. Domains with easy axes in different directions have strains which are not parallel. By constraining the material to obey certain continuity requirements, conclusions about the magnetic and deformation state of a sample may be reached. The theory of James and Kinderlehrer [5] is based on a certain energy-well structure of the anisotropy energy, consistent with crystallographic symmetry. The theory incorporates the requirement that the displacement is continuous across the domain wall, which implies that the jump in the deformation gradient is a rank-one matrix. Stable equilibrium states for an unloaded crystal are found to consist of pairs (deformation gradient, magnetization) lying at the bottoms of these energy wells which obey this rank-one condition, together with the condition that the normal component of the magnetization is continuous across interfaces in the deformed configuration. Using an energy-well structure appropriate for Terfenol-D, with easy axes on $\langle 1\ 1\ 1\rangle$ and corresponding easy strains being the measured uniaxial strains on $\langle 1\ 1\ 1\rangle$, it is found that stable laminated structures have discontinuity planes on $\{1\ 0\ 0\}$ or on $\{1\ 1\ 0\}$. Table 1 lists the magnetization directions for which each plane is associated. Discontinuities in the strain do not occur for 180° domain walls, because the magnetization is anti-parallel on either side of the wall and therefore, correspond to identical strains. To summarize, domain walls between domains of different easy axes (non-180° walls) have accompanying discontinuities in the strain. Only certain crystallographic planes are allowed to be domain walls because of the constraints on the deformation continuity in the material. These planes are listed in Table 1 along with the magnetizations they form the transition between.

To compare theory with experiment, the intersections of the planes listed in Table 1 with the (1 1 1) plane [12] are shown in Fig. 1c (oriented with the same geometry as the sample). MFM images are examined for planes of this type, and the magnetization on either side of the planes can be compared to those predicted by the theory (Table 1). For example, if the $(1\ 0\ \bar{1})$ plane is the plane of strain discontinuity, on opposite sides of this

Table 1
Planes of strain discontinuity and their associated magnetization pairs predicted by the theory [5]

Plane	Magnetization pair	Plane	Magnetization pair
(1 0 0)	[1 1 1], $[1\ \bar{1}\ \bar{1}]$	$(0\ 0\ \bar{1})$	$[\bar{1}\ 1\ 1]$, $[1\ \bar{1}\ 1]$
(0 1 1)	[1 1 1], $[\bar{1}\ 1\ 1]$	$(1\ \bar{1}\ 0)$	$[\bar{1}\ 1\ 1]$, $[\bar{1}\ 1\ \bar{1}]$
(0 1 0)	[1 1 1], $[\bar{1}\ 1\ \bar{1}]$	$(\bar{1}\ 0\ 0)$	$[1\ \bar{1}\ 1]$, $[1\ 1\ \bar{1}]$
(1 0 1)	[1 1 1], $[1\ \bar{1}\ 1]$	$(0\ 1\ \bar{1})$	$[1\ \bar{1}\ 1]$, $[\bar{1}\ \bar{1}\ 1]$
(0 0 1)	[1 1 1], $[\bar{1}\ \bar{1}\ 1]$	$(0\ \bar{1}\ 0)$	$[\bar{1}\ 1\ 1]$, $[1\ 1\ \bar{1}]$
(1 1 0)	[1 1 1], $[1\ 1\ \bar{1}]$	$(1\ 0\ \bar{1})$	$[\bar{1}\ 1\ 1]$, $[\bar{1}\ \bar{1}\ 1]$

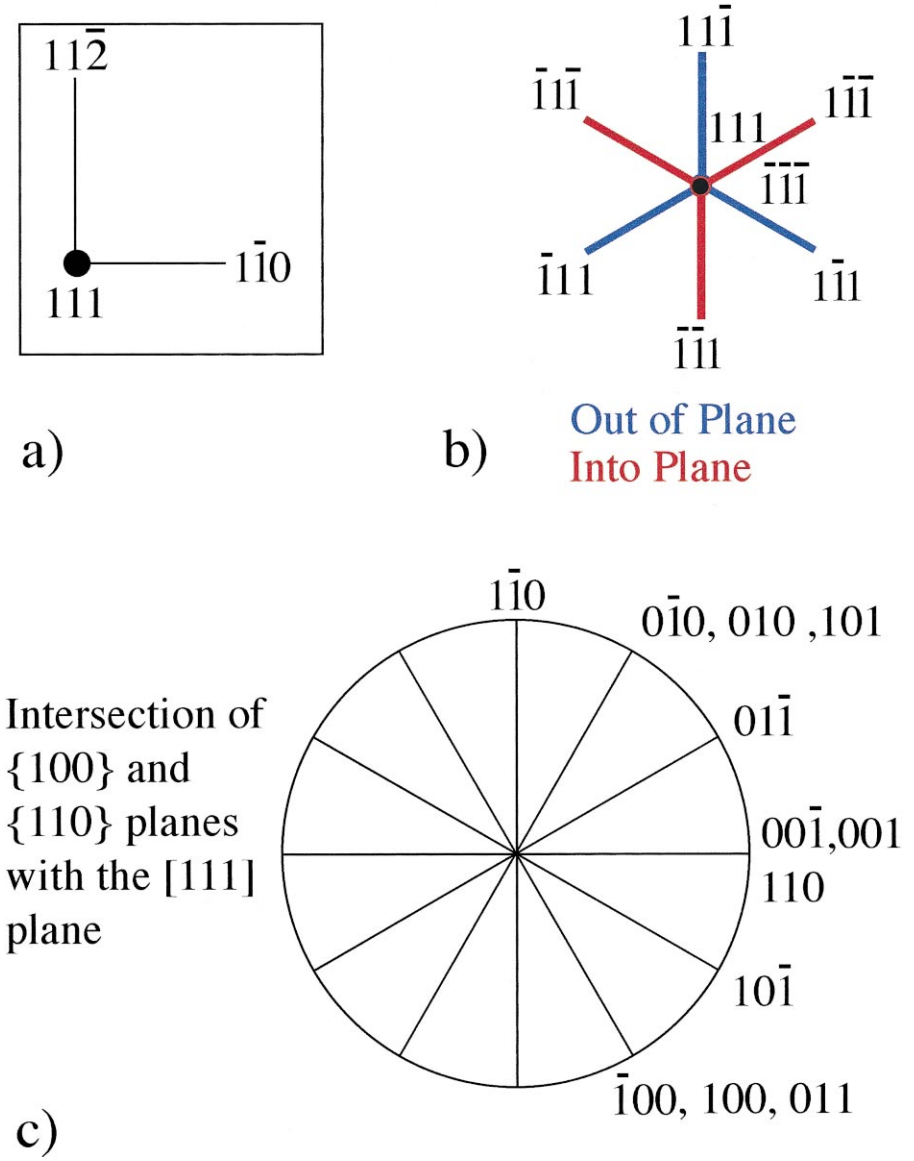

Fig. 1. (a) Top view of the geometry of both the fractured and polished samples. All images shown in this work have such a configuration, with the [1 1 $\bar{2}$] oriented vertically and the [1 1 1] easy axis pointing out of the page. The configuration of the remaining easy axes are shown in Fig. 1b. There are no fully in-plane easy axes, with half pointing into the plane, and half out of the plane. The [1 1 1] and [$\bar{1}$ $\bar{1}$ $\bar{1}$] easy axes are perpendicular to the page and the sample plane. The [1 1 $\bar{1}$], [1 $\bar{1}$ 1], and [$\bar{1}$ 1 1] axes make an angle of 19.5° with the plane. Fig. 1c shows the intersection of {1 0 0} and {1 1 0} crystallographic planes with the (1 1 1) plane.

boundary would be magnetizations in the directions of [$\bar{1}$ 1 1] and [$\bar{1}$ $\bar{1}$ 1], or their negatives. A schematic depiction of this is shown in Fig. 2b, with the addition of 180° domain walls on each side of the boundary as well.

3. Experiment/analysis

We used a Digital Instruments Dimension 3000 SPM in tapping/lift mode to perform measurements of the sample topography and magnetism.

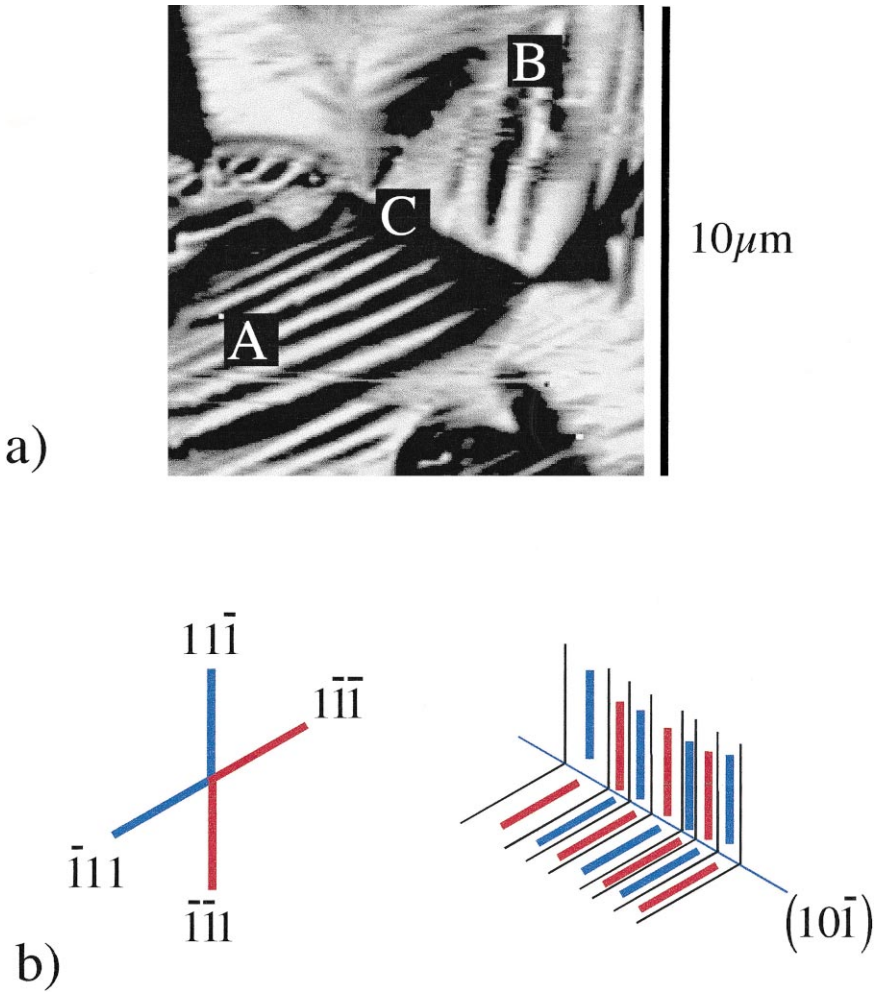

Fig. 2. (a) 10 μm MFM scan of a polished Terfenol (1 1 1) surface. Region A shows an area populated by domains of one type and region B populated by domains of a different type. These two domain types meet at the boundary marked C. (b) The easy axes associated with each region, and a schematic depiction of the magnetic structure in (a) are shown.

The probes used in this work were 225 μm long microfabricated silicon cantilevers with integrated tips sputter coated with 15 nm of Cr and 45 nm of CoCr. The magnetic field from the tip coating at the tip surface has been estimated to be $\sim$400 G [13], which appears to be sufficiently large to influence the magnetic structure of Terfenol, as seen in Fig. 2a, which shows perturbation of the magnetic structure of the sample (just below the letter B in the figure) from the influence of the scanned magnetic tip. As the tip scans across the sample plane, the magnetization of the tip may influence the sample magnetization, particularly near domain walls. This can lead to a blurred or smeared appearance of the magnetic structure. In this image and in all images presented in this work we used a cantilever and tip magnetized perpendicular to the scan plane.

Our sample was a 0.5 cm diameter rod of float zone grown Terfenol-D obtained commercially [14]. Bulk samples of Terfenol-D (easy axes: $\langle 1\,1\,1\rangle$) characteristically grow in dendritic sheets in the [1 1 $\bar{2}$] direction with growth twins in the (1 1 1) plane [2]. We polished the [1 1 $\bar{2}$] face of the

rod until the growth twins were observable under an optical microscope. The rod was then cut using an electric discharge machine in a plane parallel to the growth twin boundaries, exposing the (1 1 1) plane. The crystallographic and magnetic easy axes of the sample relative to the images shown in the paper are shown in Fig. 1a and Fig. 1b. Subsequent mechanical polishing of the (1 1 1) surface resulted in a surface flat on the nanometer scale. However, MFM images of the polished surface showed no sharp magnetic features and the boundaries between the domains were quite blurred except on the edges of the sample, where it is believed the polishing was most effective and the strain imparted was minimal. The strain from polishing was particularly important because the strains were isotropic in the plane and because of the magnetostriction, an effective in-plane anisotropy was introduced which altered the natural domain structures.

Fig. 2a shows a 10 μm MFM scan near the edge of the polished sample imaged immediately after polishing. There are a number of parallel stripe domains: one set (marked A in the figure) extends from the lower left to the upper right, and another set (marked B) is aligned close to the vertical, both of which exhibit the branched needle structure modeled by James and coworkers [15]. The domains of regions A and B meet at a line (marked C) which is oriented approximately 60° from the domains in A and B. If we identify C with a plane of strain discontinuity, we can see from Fig. 1c that it is the (1 0 $\bar{1}$) plane. Table 1 shows that the magnetization pair associated with this plane is the [$\bar{1}$ $\bar{1}$ 1] and [$\bar{1}$ 1 1]. The projections of these axes in the (1 1 1) plane are parallel to the domains marked B and A in the figure, respectively. The black and white contrast within each region is due to the domains which are along the same crystallographic axis, but change sign (the domains have a component normal to the surface which changes from parallel to anti-parallel to the tip magnetization, and vice-versa, creating contrast in the MFM image). Since the domain wall must have a normal perpendicular to the magnetization in the adjacent domains and we know the direction of the wall in the plane from the image (in the [1 1 $\bar{2}$] and [2 $\bar{1}$ $\bar{1}$] directions, for regions B and A, respectively), we can deduce the planes of the domain wall, which are (1 $\bar{1}$ 0) and (0 1 $\bar{1}$) for B and A, respectively. The magnetization of domains A and B could point along different easy axes than those proposed above and still give the same contrast in the MFM image; however, this would not satisfy the conditions of displacement continuity and strain compatibility across the domain boundaries discussed above.

Since the domains in regions A and B lie along different crystallographic axes, the strains are in different directions. The line where these meet (marked C) is a line of strain discontinuity and should be observable in the topographic scan. The topography as measured in tapping mode showed no features besides occasional pieces of detritus on the sample surface. This is likely because the sample was imaged in an as-polished state, and any topographic features associated with the strain discontinuity were likely removed. The influence of the polishing process on the magnetization could be seen not only through the blurred domain structure mentioned above, but also by the observation of virtually no magnetic domains along the [1 1 1] easy axis, which is perpendicular to the sample plane. These domains should appear to have a length scale smaller than those of the other easy axes because of the demagnetization effects associated with a larger component of the magnetization perpendicular to the sample surface. We believe that because of the nature of the mechanical polishing, there is a residual strain in the sample plane, which favors in-plane easy axes, as well as the lower magnetostatic energies associated with in-plane axes when compared to perpendicular easy axes. After demagnetization along the [1 1 $\bar{2}$] direction performed with field cycling, more [1 1 1] domains were observed which is probably due to the magnetization cycles facilitating strain relaxation of the surface.

In an attempt to eliminate effects from mechanically polishing the sample discussed above, we then followed the lead of Lord et al. [10], where clear magnetic images with very fine structure were obtained from a fracture surface. We scribed a line parallel to the (1 1 1) plane on the (1 1 $\bar{2}$) face and fractured the piece, thereby exposing the (1 1 1) plane. Although in general the fracture resulted in a rough surface, numerous regions with over

200 μm square flat areas were evident. Fig. 3 is a 75 μm MFM image of the fractured piece immediately after fracture. There are complicated domain structures with many fine features, which are characteristic of the fractured sample and are indicative of perpendicular magnetization, i.e. [1 1 1] domains. The large demagnetization energy associated with the perpendicular magnetization leads to the smaller length scale of domains. All images of the fractured surface contained domains which were predominantly [1 1 1]. This is likely because the fracture process involved pulling two planes of material apart from each other; resulting in a tensile stress perpendicular to the sample plane, which would favor domains along the stress direction, which is the [1 1 1] easy axis. Even though it was likely that there was some residual strain in the sample, it did not blur the magnetic image because all of the strain was in an easy axis direction and therefore the strain merely provided the system with a preferred easy axis.

These [1 1 1] domains are oriented into or out of plane, which show up in the image as light or dark areas of contrast. The domain walls separating the white and dark regions are 180° walls. For uncharged 180° domain walls, which have a much lower energy than charged walls, the plane of the wall must be parallel to the magnetization on each side of it. The domain walls of the [1 1 1] domains can lie anywhere in the plane. However, if the domain walls are Bloch walls, the magnetization must rotate from one easy axis to another and point in the long direction of the domain wall in the center of the wall. Taking the magnetic anisotropy into account, we can identify three different planes which would result in lower Bloch wall energies because the magnetization in the wall rotates through an easy axis. These planes are shown in Fig. 1b, and are simply the projections of the easy axes into the (1 1 1) plane. Therefore, in the images we expect to see three different kinds of domain walls which contain regions of [1 1 1] easy axis magnetization: vertical and $\pm 120^\circ$ with the vertical. Such domain walls are seen throughout the figure, although there are some domain boundaries which are not aligned with these axes.

Evidence of domain structures predicted by the theory outlined above is also present in Fig. 3. In the upper right of the image we can see very fine domains with parallel domain walls aligned nearly vertically (region 1) which all terminate along parallel lines which extend from the lower right to the upper left (marked B), which is also parallel to the line of intersection of the ($\bar{1}$ 0 0), (1 0 0), and (0 1 1) planes with the (1 1 1) plane (see Fig. 1). If we suppose that this line represents a plane of strain discontinuity, then the magnetization on either side of it must match the pair listed in Table 1. On one side of the plane we can see the [1 1 1] domains with the 180° domain walls oriented parallel to the [$\bar{1}$ 1 1] axis. We also see the very fine vertically oriented domains on the other side of the plane, whose domain walls intersect the (1 1 1) plane in a vertical line. Of the planes listed above (the ($\bar{1}$ 0 0), (1 0 0), and (0 1 1) planes), only the (1 0 0) and (0 1 1) planes have [1 1 1] easy axes as part of their magnetization pair. Both of these planes are associated with the same easy axis, since the [1 $\bar{1}$ $\bar{1}$] and the [$\bar{1}$ 1 1] are anti-parallel. The normal of the 180° domain wall separating the [1 $\bar{1}$ $\bar{1}$] and the [$\bar{1}$ 1 1] domains must be perpendicular to the magnetization in each domain and the component of the wall in the (1 1 1) plane must be perpendicular to the [1 1 1] and to the wall normal. Using these constraints, we find the domain wall to be the (3 1 2) plane. Using a similar analysis, we see the domains which make an angle of 30° with the horizontal (region 2) also consist of [$\bar{1}$ 1 1] domains which meet with [1 1 1] domains at the deformation boundaries parallel to that marked by B in the figure. The domain walls were found to be (3 2 1) planes. The fine domain structure in A can also be analyzed in exactly the same way.

To see the effects of strain on the magnetic microstructure, we epoxied a strain gage to the flat underside of the fracture piece which was mounted in the gap of a micrometer. Several small pieces of index card were placed between one end of the fracture piece and the micrometer in an attempt to ensure that the stress applied by the micrometer was approximately constant across the sample and in time. Varying stresses were applied in situ and the resulting magnetic microstructure was observed.

Fig. 4a shows a 40 μm MFM scan of a fracture surface with no applied stress. The structures on the

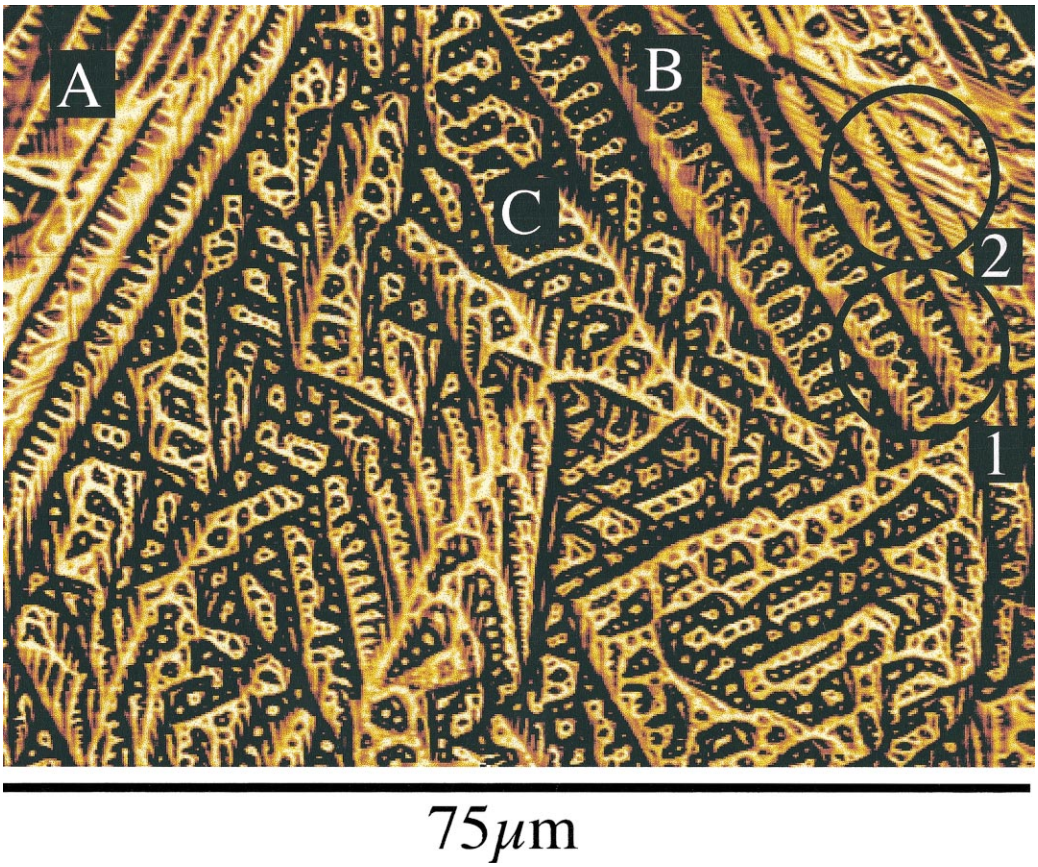

Fig. 3. Magnetic scan of a fracture Terfenol (1 1 1) surface. Regions A and B are areas where there are parallel lines (which make angles of $+30^\circ$ and -30° with the vertical, respectively) which are planes of strain discontinuity. Region C shows an area of [1 1 1] easy axis magnetization with 180° domain walls which lie along easy axis directions. The area marked 1 is an area where the planes of strain discontinuity (B) are the domain boundary between the [1 1 1] and [1 $\bar{1}$ $\bar{1}$] domains. The area marked 2 is an area where the planes of strain discontinuity (B) is the domain boundary between the [1 1 1] and [$\bar{1}$ 1 1] domains.

left side of the image are domains along the [1 1 1] easy axis, which have the characteristically smaller length scale discussed above, and have domain walls which are mostly oriented along the projections of the easy axes discussed above. In the right half of the image, there are numerous spike-like domains extending horizontally, which have a size generally larger than the domains on the left side of the image. The spikes are parallel to the intersection of the (0 0 $\bar{1}$), (0 0 1), and (1 1 0) planes with the (1 1 1) plane (see Fig. 1b). Supposing that one of these planes is a plane of strain discontinuity and that the magnetization on one side of these planes is along the [1 1 1] easy axis, Table 1 shows that either the (0 0 1) or the (1 1 0) has a [1 1 1] easy axis in the magnetization pair. The other member of the pair is either [1 1 $\bar{1}$] or [$\bar{1}$ $\bar{1}$ 1] which are antiparallel and have projections into the plane vertically in the image. If we look above one of the spikes, e.g. in the white box in Fig. 4a, we can see small domains which may be aligned along the [1 1 $\bar{1}$] direction, or they could be [1 1 1] domains. Also seen below each spike is a dark area in which are embedded many small light domains, which have the characteristics of the [1 1 1] domains on the right side of the image. If this black area is interpreted as being magnetically aligned with the [1 1 1], the plane of discontinuity may be at the

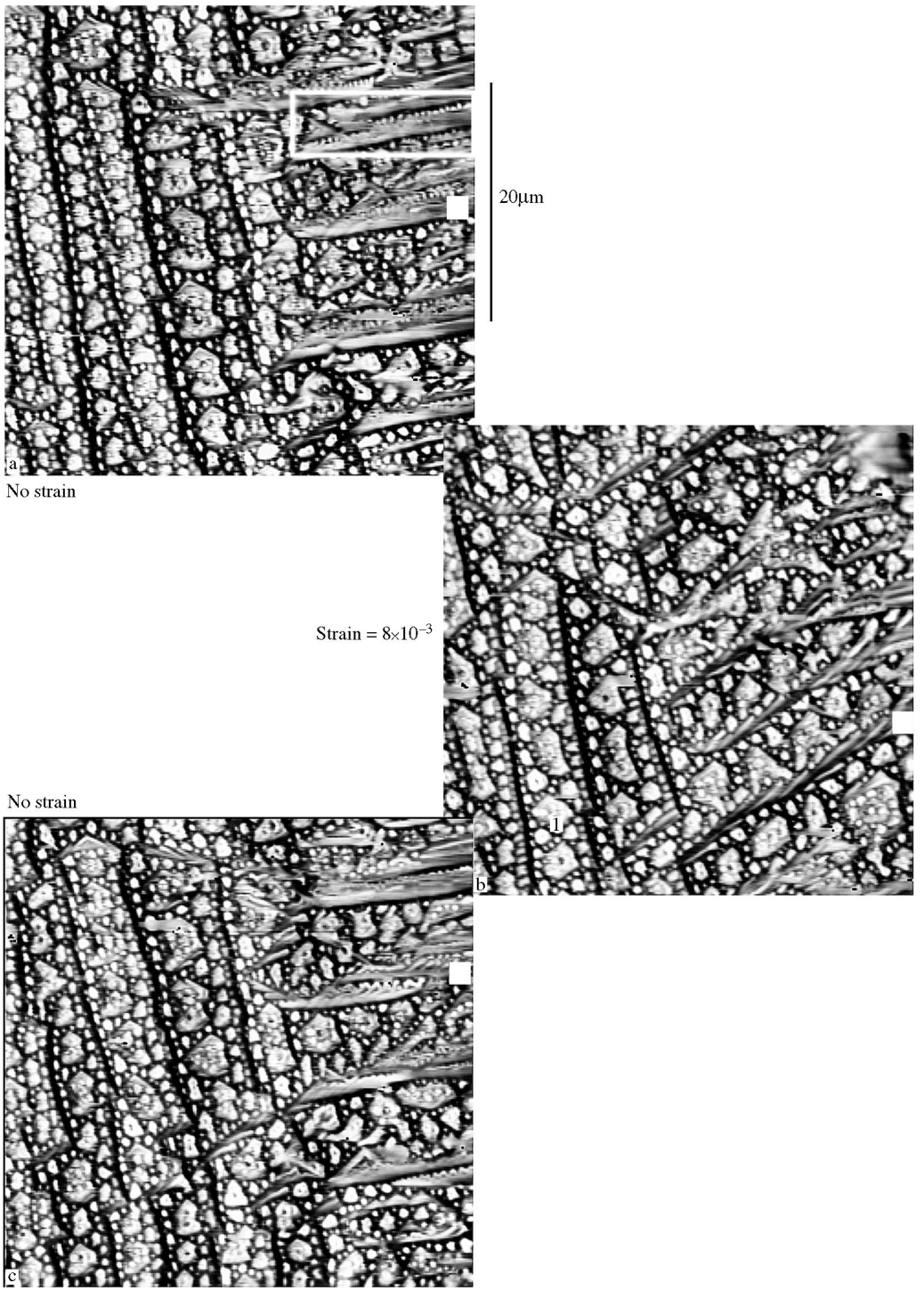

Fig. 4. A sequence of 40 μm MFM images of the fracture (1 1 1) surface of Terfenol-D with in situ applied stress, (a) with no applied stress. Contained in the white outline are boundaries between domains with [1 1 1] and [1 1 $\bar{1}$] easy axis magnetization; (b) has a strain of 8×10^{-3}. Region 1 in (b) denotes a region of [1 1 1] easy axis magnetization which has exhibited domain wall motion resulting from the stress application; (c) with no stress applied and displays magnetic hysteresis. The white square marks the same topographic location on the sample.

boundary between the dark and light regions, implying that the light colored area is a single domain aligned along the [1 1 $\bar{1}$]. The small domains in the white box mentioned above would then be the single [1 1 $\bar{1}$] domain breaking up into smaller domains separated by 180° walls in an effort to minimize the magnetostatic energy, or the top of the solid white spike could be another plane of strain discontinuity and the small domains would then be [1 1 1] domains.

As compressive stress along the [1 1 $\bar{2}$] axis is applied (vertically in this image), the domain structure of the sample changes (Fig. 4b). The strain in the sample measured during this image is 8×10^{-3}. The most noticeable changes involve the spike domains on the right side, which have transformed into wedges which point in a direction approximately 30° below horizontal (parallel to the projection of the [$\bar{1}$ 1 1] axis in the plane). The [$\bar{1}$ $\bar{1}$ 1] easy axis, as discussed in the Theory section, is the axis which is the most prone to change under a compressive stress applied along the [1 1 $\bar{2}$] axis. Since this is so, we would expect to see the [$\bar{1}$ $\bar{1}$ 1] easy axis domains to disappear, either through the growth of the [1 1 1] domains which surround them, or through rotation of the magnetization of the domain into a different easy axis. It appears that the [$\bar{1}$ $\bar{1}$ 1] domains rotated into a [$\bar{1}$ 1 1] easy axis. Some remnants of the horizontal deformation planes remain, but the domain walls parallel to the projection of the (0 1 $\bar{1}$) plane may indicate that the energetically unfavorable [$\bar{1}$ $\bar{1}$ 1] domains are transforming into [1 $\bar{1}$ 1] domains via the (0 1 $\bar{1}$) deformation discontinuity plane.

On the left half of the image (Fig. 4b) we can also see the effects of stress on the [1 1 1] easy axis domains. In general, any application of compressive stress similar to that applied in our experiment would result in the sample becoming entirely magnetized in the [1 1 1] easy axis direction, for large enough stresses. Since the magnetization of the majority of the images in Fig. 4 is already in the [1 1 1] direction, there is not much growth possible for these domains. However, we do observe the large area of light contrast (marked 1 in the figure) becoming slightly wider, and generally the long vertical domains breaking up into shorter segments. This is a consequence of the orientation of the domain walls which run nearly vertically in the figure. The magnetization inside these domain walls is in the [$\bar{1}$ $\bar{1}$ 1] direction at the center, and so is highly energetically unfavorable under a compressive stress applied in the manner of our experiment. To minimize this energy, the domain wall can break up into shorter segments, with more of the domain perimeter consisting of walls in other easy axis directions, or the domains can get wider, which means that fewer of the vertically oriented walls are required. Both mechanisms appear to be at work in Fig. 4b.

Fig. 4c shows a scan of the same sample area after the applied stress has been removed. Although the strain of the sample during the image is the same as in Fig. 4a, the sample magnetism clearly shows hysteresis. The [1 1 1] easy axis domains on the left half of the image are a combination of those found in Fig. 4a and Fig. 4b; the domain walls have returned to a more vertical configuration, but the widening of the domains which took place in Fig. 4b appears to have remained. The horizontal spike domains have returned and the wedges oriented at 30° to the horizontal are gone for the most part although a few remain.

4. Conclusions

We have imaged the (1 1 1) surface of polished and fractured Terfenol-D. The observed magnetic structure is in general quite complicated, although many of the domain configurations observed were able to be explained through application of the theory of James and Kinderlehrer [5]. The effects of magnetostriction were seen in the variation of the magnetic domain types with the strain history of each sample. Magnetostrictive effects were also seen when the Terfenol was imaged during in situ stress application.

Acknowledgements

This research was supported by grants #N00014-94-1-0123 and #N00014-95-1-0799 from the Office of Naval Research. One of the authors (J.S.) would like to thank the University of Minnesota graduate school for financial support.

References

[1] D.G. Lord, D. Harvey, J. Appl. Phys. 76 (1994) 7151.
[2] A.E. Clark, J.D. Verhoven, O.C. McMasters, E.D. Gibson, IEEE Trans. Magn. 22 (1986) 973.
[3] A.E. Clark, J.P. Teter, O.D. McMasters, J. Appl. Phys. 63 (1988) 3910.
[4] W.D. Armstrong, J. Appl. Phys. 81 (1997) 3548.
[5] R.D. James, D. Kinderlehrer, Phil. Magn. B 68 (1993) 237.
[6] D.G. Lord, V. Elliott, A.E. Clark, H.T. Savage, J.P. Teter, O.D. McMasters, IEEE Trans. Magn. 24 (1985) 1716.
[7] J.P. Teter, K. Mahoney, M. Al-Jiboory, D.G. Lord, O.D. McMasters, J. Appl. Phys. 69 (1991) 5768.
[8] M. Al-Jiboory, D.G. Lord, Y.J. Bi, J.S. Abell, A.M.H. Hwang, J.P. Teter, J. Appl. Phys. 73 (1993) 6168.
[9] A.P. Holden, D.G. Lord, P.J. Grundy, J. Appl. Phys. 79 (1996) 4650.
[10] D.G. Lord, A.P. Holden, P.J. Grundy, J. Appl. Phys. 81 (1997) 5728.
[11] A.P. Holden, D.G. Lord, P.J. Grundy, J. Appl. Phys. 79 (1996) 6070.
[12] E.A. Wood, Crystal Orientation Manual, Columbia University Press, New York, 1963.
[13] D.G. Streblechenko, M.R. Scheinfein, M. Mankos, K. Babcock, IEEE Trans. Magn. 32 (1996) 4124.
[14] Etrema Products Inc., Ames, Iowa, USA.
[15] R.D. James, R.V. Kohn, T.W. Shield, J. de Physique IV Colloque C 8 5 (1995) 253.